State of Charge Management for Grid-Connected PV with Supercapacitor System Considering LVRT Operation

Paychuda Kritprajun
Department of Electrical Engineering and Computer Science
The University of Tennessee
Knoxville, TN, USA
pkritpra@vols.utk.edu

Leon M. Tolbert
Department of Electrical Engineering and Computer Science
The University of Tennessee
Knoxville, TN, USA
tolbert@utk.edu

Jingjing Sun
Department of Electrical Engineering and Computer Science
The University of Tennessee
Knoxville, TN, USA
jsun30@vols.utk.edu

Jingxin Wang
Department of Electrical Engineering and Computer Science
The University of Tennessee
Knoxville, TN, USA
jwang78@utk.edu

Nattapat Praisuwanna
Department of Electrical Engineering and Computer Science
The University of Tennessee
Knoxville, TN, USA
npraisu1@vols.utk.edu

Yunting Liu
Department of Electrical Engineering
The Pennsylvania State University
University Park, PA, USA
ypl5778@psu.edu

Maximiliano Ferrari
Grid Components and Control
Oak Ridge National Laboratory
Oak Ridge, TN, USA
ferrarimagmf@ornl.gov

2023 IEEE Energy Conversion Congress and Exposition (ECCE) | 979-8-3503-1644-5/23/$31.00 ©2023 IEEE | DOI: 10.1109/ECCE53617.2023.10362220

***Abstract*— This paper presents a state of charge (SOC) management strategy to ensure low-voltage ride-through (LVRT) services of a grid-connected photovoltaic (PV) with a supercapacitor (SC) energy storage system (PVSS). A concept of SOC reservation for LVRT operations is introduced to guarantee that the PV grid-connected system can provide LVRT services complying with grid code requirements. SOC management is derived by considering SC limitations, the current rating of the converters, and grid conditions. Therefore, safe operation of the power system and PVSS can be achieved. The study also adopts an electrothermal model of the SC to adjust the current set points during SOC management by considering the temperature-dependent SC parameters; thus, both safety and full utilization of the SC can be achieved. Consequently, SOC management can rapidly be accomplished, thereby increasing the certainty of providing LVRT services to the system.**

Keywords—Grid-connected photovoltaic system, supercapacitor, low-voltage ride-through, state of charge management

I. INTRODUCTION

Research in power management of grid-connected photovoltaic (PV) with energy storage systems (ESS) has been increasing due to their efficiency improvement and cost reduction [1]. A supercapacitor (SC) is one of the ESS technologies gaining more interest currently in PV systems integrated with energy storage systems, either as a standalone [1]–[3], or as part of a hybrid system with battery [4], [5] due to its fast response and high power capacity [6]. During grid fault events, SC is used to absorb excess power on the dc-link when the PV system cannot inject power to the grid and to provide power to the local load when the grid power is insufficient [3], [7]. With the support of the SC during faults, PV curtailment with limited ramp rate capability can be avoided. Thus, there are less dc-link overvoltage issues [3], [7] and the PV system can continue to operate in maximum power point mode.

State of charge (SOC) management is used to maintain the availability of SC operation due to its limited energy capacity. The SOC also needs to be controlled within the range according to the maximum and minimum of the SC's voltage. The SOC's upper limit is associated with the maximum SC voltage specified in the datasheet to prevent overcharging the SC. The SOC's upper limit can be set lower than its rating to prolong the SC's lifetime [8]. In the case where the SC is connected to a buck-boost dc-dc converter, the minimum SOC is determined by the minimum input voltage requirement of the converter to maintain the converter's ability to regulate the dc-link voltage.

SC availability is the main concern, especially during grid disturbances when the SC is used to maintain the PV system's stability [7]. Ref. [1] proposed SOC management for fault ride-through (FRT) operations considering the time required during FRT operation and the SC capacity. The SOC management according to [1] will be activated if the SOC reaches its limits (upper limit of 90% or lower limit of 60%), and the SOC will be restored to 80% or 70%, respectively. Considering the way to restore the SOC, the maximum fixed capacity at 10% of the SOC is reserved for the LVRT operation in this literature. However, the fixed SOC reserve band might be limited only to a grid-connected SC system in the literature, but not for the hybrid system with variations of PV and load.

The power reference of SOC management is determined depending on several factors such as power rating, SOC level, and grid condition. A factor of 25% to 30% of the maximum power rating is used as a power reference during SOC management in [1], [9], [10], but the reason behind choosing those percentages is not provided in the literature. Because the full power capacity is not utilized, the time required for SOC management can be longer than it should be. SOC level is considered as a factor to determine the reference current during SOC management in [9], [11]. This method has a disadvantage if the SOC level between its target and the current SOC is low;

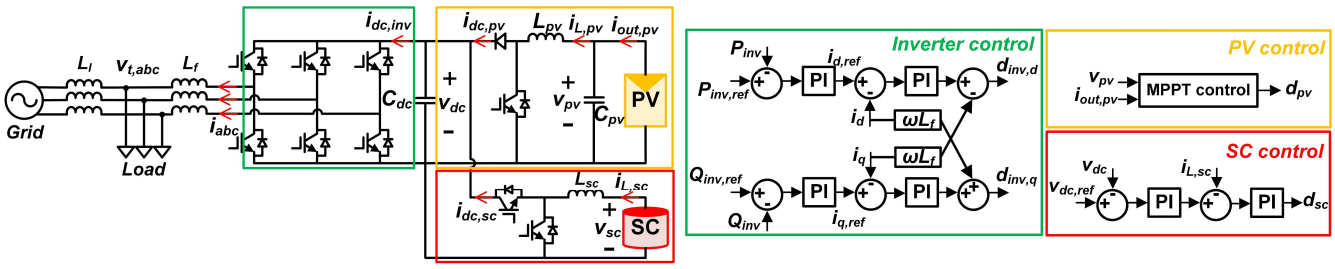

(a) Circuit diagram of the PVSS.

(b) Control diagrams of the inverter, PV system, and SC system in the PVSS.

Fig. 1. The circuit diagram and control of the grid-connected PV with SC system (PVSS) [12].

it will result in a low power reference during SOC management. Thus, a longer time will be required to restore the SOC to the target value. The grid voltage is employed as a function to enable and disable SOC management in most literature [1], [9], [10]. However, this approach can introduce an issue with the constant power during the SOC management. This constant power reference can act as a step change based on the grid voltage, causing oscillation issues on the grid voltage due to power fluctuations when the grid voltage is close to the boundaries that trigger the SOC management actions.

The main contributions of this paper are as follows: 1) The concept of a dynamic SOC reservation band is introduced for LVRT operations considering PVSS operating conditions. 2) A revised SOC management is proposed by considering grid conditions rather than a disable/enable function based on grid voltage to avoid oscillation in the grid voltage due to the power fluctuations during SOC management. 3) Allowable current adjustment is based on a SC thermal model to maximize the SC capacity during SOC management. Thus, the proposed SOC management with SOC reservation concept can achieve a shorter SOC management time rather than the traditional fixed power reference, while ensuring safe operations of both the grid and PVSS.

II. Grid-connected PV with SC System [12]

The circuit diagram of a grid-connected PV with supercapacitor system (PVSS) is shown in Fig. 1. The PVSS consists of a PV with its interface dc-dc boost converter, SC with its bidirectional dc-dc buck-boost converter, and a grid-connected inverter. More details of the PVSS model and its control can be found in [12], and the PVSS's parameters are provided in Table I.

A. Supercapacitor System

This paper adopts the Zubieta model to represent the SC's dynamics in the study. The model has a good compromise between complexity and accuracy for short-term and long-term simulations, thus it is suitable for power system studies [13].

An average current control is adopted to control the SC's bidirectional buck-boost dc-dc converter operations as shown in Fig. 1(b). The dc-link voltage is regulated by controlling the amount of charge and discharge current of the SC in buck and boost operations, respectively [14], [15]. The control is achieved by PI controllers; the control parameters are presented in Table I.

B. PV System

In normal operation mode, PVSS injects PV power to the grid according to the solar irradiation. The PV system is controlled in maximum power point (MPP) mode by using the perturb and observe (P&O) method adopted from [16]. The duty cycle of the PV's boost dc-dc converter is adjusted to move the PV's operation toward its MPP based on the changes in the PV power and the PV voltage from the previous operation. The next PV operation can be determined by the P&O control diagram [12], [16] presented in Fig. 2.

C. Grid-connected Inverter

The control of a grid-connected inverter is achieved in dq coordinates by implementing a common cascade control structure [17]. Active and reactive powers are controlled by the outer loop PI controllers. The inner loop PI controllers are used to control the inverter's current based on the references generated by the outer power control loops. The control diagram of the grid-connected inverter is presented in Fig. 1(b).

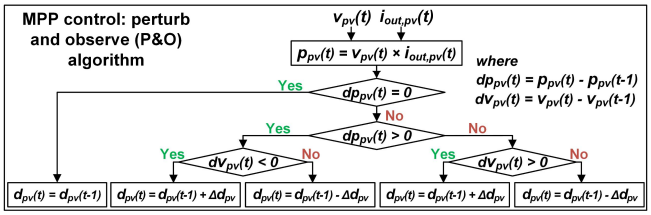

Fig. 2. MPP control of the PV's dc-dc converter based on the P&O algorithm [12], [16].

TABLE I. PVSS's Parameters [12].

SC's Parameters	**Values**
SC capacitance (C_{sc})	16.67 F
Voltage rating ($v_{sc,raing}$)	486 V
Dc-dc converter rating ($P_{sc,rating}$)	55 kW
Dc-dc converter's inductor (L_{sc})	0.4 mH
Dc-link voltage PI controller	$k_{p,v}$ = 1.579, $k_{i,v}$ = 464.4
Current PI controller	$k_{p,i}$ = 0.002396, $k_{i,i}$ = 8.557
PV's Parameters	**Values**
Power rating ($P_{pv,rating}$)	50 kW
Dc-dc converter's input capacitor (C_{pv})	100 µF
Dc-link's Parameters	**Values**
Voltage rating (v_{dc})	900 V
Dc-link capacitor (C_{dc})	1500 µF
Inverter's Parameters	**Values**
Power rating ($S_{inv,rating}$)	55 kVA
Inductor filter (L_f)	0.5 mH
Line inductance (L_l)	2.3 mH
Outer loop active and reactive powers PI controllers	$k_{p,pq}$ = 2.871, $k_{i,pq}$ = 57419
Inner loop currents PI controllers	$k_{p,i-dq}$ = 0.052, $k_{i,i-dq}$ = 22.75

III. PVSS DURING LVRT OPERATIONS

During LVRT events, the PVSS is required to stay connected to the grid and provide voltage support according to the grid requirements. This study adopts the reactive power-voltage (Q-V) droop curve based on IEEE 1547-2018 [18] with the maximum reactive power capacity based on the PVSS's power rating to support the grid during LVRT events. The change of reactive power (ΔQ_{sup}) to support the grid voltage during LVRT operations can be calculated as follows [12], [18]:

$$\Delta Q_{sup} = k_{vq}\Delta v \tag{1}$$

where k_{vq} = 20 is the coefficient of the reactive power-voltage control loop, which is associated with 5% droop. Δv is the change in voltage during the LVRT event compared to the deadband of the grid voltage [18].

IV. SOC MANAGEMENT CONSIDERING LVRT OPERATION

A. SOC Reservation Concept for LVRT Operation

SC normally absorbs or provides its power in order to maintain the power balancing between the dc-side and grid side to regulate the dc-link voltage. During the LVRT event, the power imbalance tends to increase due to the low voltage condition of the grid limiting the amount of injected power. The SC should have sufficient capacity to support the system by absorbing the power from the PV that cannot be injected into the grid.

The concept of SOC reservation is to estimate the amount of SC capacity that will be used during a LVRT event so that the SC capacity can be reserved to ensure its availability during LVRT services. The proposed SOC reservation band (SOC_{lvrt}), which indicates the estimated final value of the SOC after the LVRT event, can be calculated according to the PVSS operating conditions as follows:

$$\begin{aligned} P_{sc,lvrt} \times t_{lvrt} &= 0.5C_{sc}\left(v_{sc,lvrt}^2 - v_{sc}^2\right) \\ SOC_{lvrt} &= SOC + \frac{(v_{sc,lvrt} - v_{sc})}{v_{sc,\text{rating}}} \end{aligned} \tag{2}$$

SOC_{lvrt} can be higher or lower than the current SC's SOC (SOC) depending on whether the SC will absorb or inject power during a LVRT event. The SOC reservation band is represented by the $(v_{sc,lvrt} - v_{sc})/v_{sc,\text{rating}}$ term in (2). v_{sc} is the SC voltage, and $v_{sc,lvrt}$ is the estimated SC voltage after the LVRT event as determined from the calculation. The time duration (t_{lvrt}) is selected to be 5 s, which is the maximum time required for mandatory LVRT operations, based on Category II in IEEE 1547-2018 [18]. The estimated SC power ($P_{sc,lvrt}$) during LVRT operation is the unbalanced power at the dc-link between the PV output power and the critical local load's power that will be provided by the SC during the LVRT event.

When the PV generation is greater than the critical load, the SOC_{lvrt} will be higher than the SOC. This indicates that if the LVRT event happens, the SC will need to absorb the remaining PV power after supplying power to the critical load during the LVRT event. Also, the PVSS will provide reactive power based on the available reactive power capacity to improve the grid voltage. This operation is depicted in Zone 1 in Fig. 3.

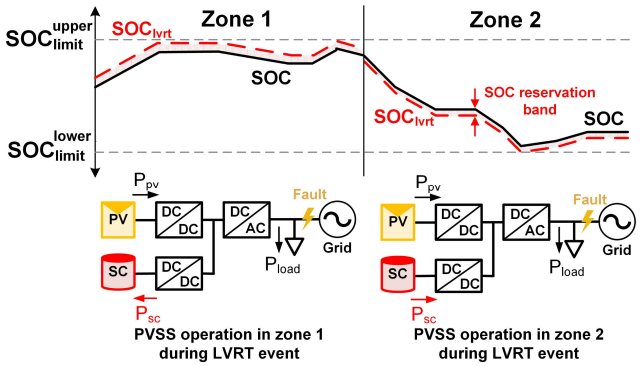

Fig. 3. SOC reservation concept.

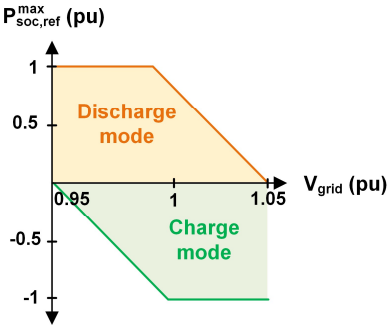

Fig. 4. Active power-voltage curve for SOC management.

Another PVSS operation is when the PV power is lower than the critical load as presented by Zone 2 in Fig. 3. In this case, the SC will provide the power to support the critical load during the LVRT operation when the grid power is not available. So, the SOC_{lvrt} in this case will be lower than the SOC, which means the SC's capacity will be reduced during the LVRT event from supplying power to the load.

The SOC_{lvrt} is used to activate the SOC management to reserve the SC's capacity for supporting the PVSS during LVRT operation. An advantage of the proposed SOC reservation concept is a dynamic band according to the PVSS operating conditions, rather than assuming that the SC capacity will be used within a certain amount [1] that could be larger or smaller than it should be. This avoids unnecessary SOC management that interrupts the SC operations while ensuring SC availability to support the LVRT event.

B. SOC Management Considering Grid Conditions

To incorporate the grid conditions while restoring the SC's SOC, the relationship is established between grid voltage and active power reference by adopting the active power-voltage (P-V) droop curve similar concept to IEEE 1547-2018 [18]. However, the droop curve adopted in this paper is revised for SOC management, where the operating voltage during the management will be limited within the grid voltage deadband to avoid violating the grid condition. The power reference during the SOC management will be adjusted according to the grid voltage rather than using a fixed power reference as done in [1], [9], [10]. Thus, SOC management can be achieved while maintaining the grid voltage within safe limits.

The maximum grid side power reference ($P_{soc,ref}^{max}$) during SOC management when considering grid conditions as shown in Fig. 4 can be calculated as follows.

$$P_{soc,ref}^{max} = k_{vp}\left(v_{grid,lim} - v_{grid}\right) + P_{grid,int} \quad (3)$$

where $v_{grid,lim}$ is the grid voltage (v_{grid}) limits between 1.05 pu and 0.95 pu and $P_{grid,int}$ is the active power of PVSS before the SOC management. k_{vp} is the coefficient of the active power-voltage control loop at 20.

The $P_{soc,ref}^{max}$ will be used as one of the factors to determine the power reference ($P_{inv,ref}$) during the SOC management. Other factors including the SC thermal capacity, SC current, and converter's capacity will be discussed in the next section.

SOC management will be enabled only when the SOC_{lvrt} is outside the limits (upper limit at 90% and lower limit at 40%) and grid voltage is within the limits. The target SOC_{lvrt} value of the SOC management for this paper is 65%, which is the middle of the SOC working range. This number is set by considering the equivalent possibility of the SC to be in charging or discharging modes.

V. SC Current Adjustment Based on Temperature

This section presents the models used to incorporate the SC thermal capacity into the SOC management function so that the SC capacity can be fully utilized while ensuring its safe operation. The details are provided in the following sections.

A. SC's Equivalent Series Resistance (R_{ESR}) Model

The SC's equivalent series resistance (R_{ESR}) is greatly impacted by the SC temperature, thus it should be properly modeled based on the operating temperature [19]. This paper adopts the R_{ESR} model from [19], [20], in which the R_{ESR} of the SC cell according to its temperature (T) can be calculated as follows:

$$R_{ESR} = b_1 R_{ESR,0}\left(1 + \gamma(T - T_0)\right) + b_2 R_{ESR,0}(\exp(-0.5 k_T (T - T_0))) \quad (4)$$

where $R_{ESR,0}$ is 0.23 mΩ based on the temperature (T_0) at 25 ºC given in the SC datasheet [21]. The electronic (b_1) and ionic (b_2) weight factors at 0.55 and 0.45, respectively. The coefficient of resistance sensitivity to temperature (γ) is 0.007, and the Arrhenius factor of ionic temperature dependence (k_T) is 0.045 [19], [20].

The updated R_{ESR} to the SC thermal model will increase the estimation accuracy of the SC cell temperature. Consequently, the SC current reference can be properly adjusted according to the SC temperature.

B. SC Thermal Model

This study adopts the string thermal model of the SC [22], [23], [25] to estimate the SC temperature based on its operation. The SC cell temperature will be used as an input of the SC current adjustment function to adjust the SC current based on its thermal capacity so that the SOC management time can be shorter, thus the SC can be ready for the next operation shortly.

The adopted SC thermal model is based on the inline arrangement. This thermal model can be simplified by assuming that the mass flow rate from one node to another one is similar for all consecutive nodes [24]. Thus, the thermal network model of the SC stack for the inline arrangement can be reduced to a string thermal network [22], [24] as shown in Fig. 5.

The heat generation (Q) for the SC string thermal model is approximated by the power loss ($i_{L,sc}^2 R_{ESR}$) [22]. The heat exchange between the SC's core and its surface is modeled by the heat conduction over a conduction resistance (R_c). While the heat transfer between the surface and ambient is modeled by using a convection resistance (R_u) [25].

The SC temperatures, where there are n cells in the SC string can be calculated as follows [22], [23], [25].

$$\begin{aligned} C_c \frac{dT_{c,n}}{dt} &= i_{L,sc}^2 R_{ESR} - \frac{(T_{c,n} - T_{s,n})}{R_c} - \frac{(T_{c,n} - T_{c,n-1})}{R_{cc}} - \frac{(T_{c,n} - T_{c,n+1})}{R_{cc}} \\ C_s \frac{dT_{s,n}}{dt} &= \frac{(T_{c,n} - T_{s,n})}{R_c} - \frac{(T_{s,n} - T_{f,n})}{R_{u,n}} \\ T_{f,n} &= T_{f,n-1} + \frac{(T_{s,n-1} - T_{f,n-1})}{R_{u,n} C_f} \end{aligned} \quad (5)$$

where T_c is SC cell core temperature, T_s is SC cell surface temperature, T_f is ambient temperature, with all temperatures in Kelvin. $T_{f,n}$ at the nth cell can be calculated by the heat balance equation related to the heat flow [22]; where the generated heat at the ambient node ($Q_{f,n}$) is the summation of the heat taken from the $(n-1)$th cell by the convection and the heat transferred from the previous ambient node ($Q_{f,n-1}$). R_u is greatly affected by the airflow pattern, turbulence, and velocity [22]; thus, their values vary based on the cell's location with respect to the airflow source. Since the kinetic energy of the airflow will eventually reach the steady value in one location, the cells starting from that location will have the similar R_u [22]. More details of the thermal mode implemented in this paper can be found in [22], [23], [25]. Other parameters in (5) are referred from [22]–[24], and their values are provided in Table II.

The airflow of the SC string thermal model is from SC cell number $n-1$ to n. Thus, the SC cell with the highest temperature will be the last one in the SC string since it's the farthest from the airflow source.

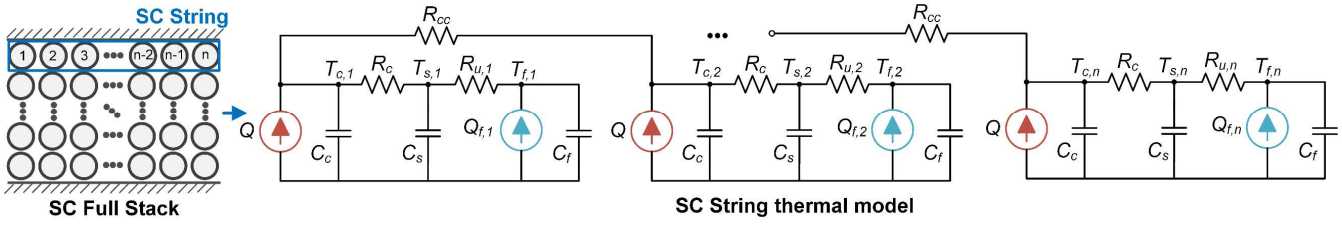

Fig. 5. SC string thermal model [22], [23], [25].

TABLE II. SC'S THERMAL PARAMETERS [22]–[24].

Parameters	Values
Cell to cell conduction resistance	R_{cc} = 21.99 KW^{-1}
Conduction thermal resistance	R_c = 0.627 KW^{-1}
Convection thermal resistance	$R_{u,1}$ to $R_{u,4}$ = 1.38 KW^{-1} $R_{u,5}$ to $R_{u,20}$ = 2.4 KW^{-1}
Thermal capacity corresponding to the internal elements	C_c = 700 JK^{-1}
Thermal capacity corresponding to the casing elements	C_s = 7 JK^{-1}
Cooling air heat capacity based on the cooling fan speed at 34.1 CFM	C_f = 18.45 JK^{-1}s^{-1}

C. SC Current Adjustment based on SC's Temperature

Due to the need for quick SOC management, higher current operation is preferred to reduce the SOC management operating time. The SC can operate at a high current based on its current limit determined by the voltage and R_{ESR} as described in [26]. However, the main concern of high current operation is related to the temperature rise in the SC cell according to its operation that can lead to thermal runaway.

The study incorporates the SC cell temperature from the SC thermal model given by [22], [23], [25] so that the SC current can be adjusted based on its thermal limitations [26] in order to maximize the SC capacity. The SC current reference ($I_{temp,ref}$) when considering the SC thermal capacity can be calculated as follows [26].

$$I_{temp,ref} = \frac{T_{max} \times \sqrt{\frac{\Delta T}{R_{ESR} \times R_{u,sc}}}}{T_{sc}} \quad (6)$$

where T_{sc} and R_u are the temperature of the last SC cell in the SC string thermal model and its convection thermal resistance. Because the inline arrangement of the SC string with the airflow direction from the first cell to the last cell, the last SC cell will have the highest temperature. T_{max} is the maximum allowable SC cell temperature provided in the SC datasheet. ΔT is the difference between T_{max} and the ambient temperature.

The power reference during the SOC management can be determined according to Algorithm 1, which incorporates the thermal capacity of the SC, grid conditions, and the limits of the PVSS's converters presented in the above sections.

VI. EXPERIMENTAL SETUP OF PVSS

The experimental tests are performed on a grid emulation hardware testbed (HTB) platform, where multiple voltage source converters (VSCs) can be emulated as grid components to form the system under test [15]. A digital signal processor (DSP) model TMS320F28335 from Texas Instruments is used as a microprocessor for each emulator that includes the grid component's model and control.

As shown in Fig. 6, the experimental setup uses three VSCs to form the system under test including generator emulator [27], load emulator [28], and PVSS emulator [12]. The emulators on the HTB are connected on the ac-side through the line inductance (L_l) allowing the power flow between emulators similar to the flow between grid components in real systems. More details on the setup can be found in [12] and the PVSS's model parameters used in the emulator are provided in Table. I.

Algorithm 1: Power reference during the SOC management

Input:
$I_{temp,ref}$: current reference according to the SC thermal capacity from (6)
v_{sc}: SC's voltage
$P_{soc,ref}^{max}$: the maximum grid-side power reference considering grid condition from (3)
Output:
$P_{inv,ref}$: the inverter's power reference during the SOC management
Procedure:
Compute $P_{sc,ref} = I_{temp,ref} v_{sc}$;
if $P_{sc,ref} > P_{sc,rating}$
  $P_{sc,ref} = P_{sc,rating}$; *// limit the SC power based on its dc-dc converter rating*
end
Compute $P_{inv,ref} = P_{pv} + P_{sc,ref}$; **and** $P_{ac,avi} = \sqrt{S_{inv,rating}^2 - Q_{inv}^2}$;
if $P_{inv,ref} > P_{ac,avi}$;
  $P_{inv,ref} = P_{ac,avi}$; *// limit the active power reference based on the available active power of the inverter*
end
if $P_{inv,ref} > P_{soc,ref}^{max}$
  $P_{inv,ref} = P_{soc,ref}^{max}$; *// limit the active power reference of the inverter based on the maximum grid-side power reference considering grid condition*
end

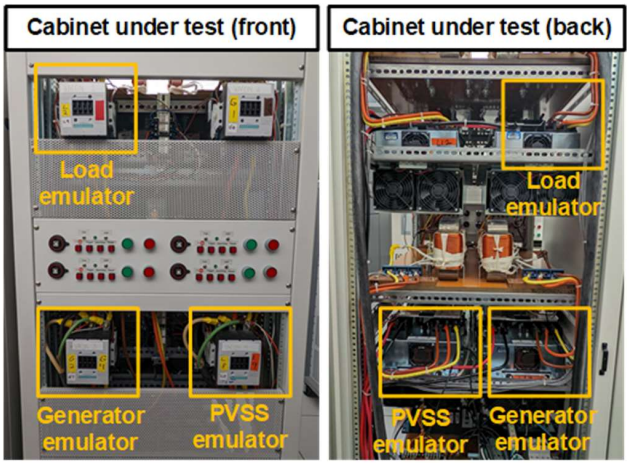

Fig. 6. Experimental test setup of the PVSS on the HTB [12].

VII. EXPERIMENTAL RESULTS

A. Results of PVSS Operation during a LVRT Event

The short-term low voltage event when the grid voltage drops to 0.58 pu is emulated to demonstrate the PVSS operation during the LVRT event.

As shown in Fig. 7 when the LVRT event starts, the PVSS provides reactive power to increase the grid voltage to 0.67 pu during the disturbance. Meanwhile, the SC quickly absorbs the PV power at 50 kW in order to reduce the unbalanced power on the dc-link. There are some dc-link voltage oscillations during the transition between the normal mode and LVRT operation, yet the dc-link voltage can be regulated at its nominal value due to the fast response of the SC. Thus, the PVSS can remain connected to the grid during this low-voltage event while the PV system continues its operation in the MPP mode. The stored PV power in the SC during the LVRT event can be injected into the grid later when the system is back to normal operation.

B. Results of SOC Reservation for LVRT Operation

In this section, the performance of the SOC reservation concept is demonstrated, and it is compared to the traditional SOC management for the LVRT operation based on [1].

For this LVRT scenario as shown in Fig. 8, two consecutive LVRT events are emulated. The PVSS operates at 40 kW with no load and the SC's SOC is at 80% before the LVRT operations. This test represents the worst-case scenario, where the LVRT event's duration is 5 s for each operation and the time between these two LVRT events is 10 s.

During the 1st LVRT event, the PVSS can remain connected to the grid and provide reactive power to increase the grid voltage, complying with the grid requirements for both traditional [1] and the proposed methods. For the proposed method, the SOC after the 1st LVRT event is equal to the SOC_{lvrt} before the LVRT operation, which verified that the estimation accuracy of the SC capacity used during the event was properly reserved. After the 1st LVRT event when the grid voltage is back within its operation range, the SOC management of the proposed method is activated due to the SOC_{lvrt} is higher than its limit as shown in Fig. 8(a). Meanwhile, the SOC management of the traditional method [1] as presented in Fig. 8(b) is not activated because the SOC has not yet reached its limit at 90%.

The SOC management of the proposed method is designed to stop when the SOC_{lvrt} reaches the target value at 65%. However, it is interrupted by the 2nd LVRT event that happens after the 1st LVRT operation is completed by 10 s. Since the power during the SOC management of the proposed method was maximized according to the SC thermal capacity, the SOC_{lvrt} of the proposed method is lower than 90% before the 2nd LVRT operation. This indicates that the SC has sufficient capacity to support the 2nd event based on the current PVSS operation. Consequently, the PVSS can remain connected to the grid, and it can provide voltage support while regulating its dc-link voltage throughout the 2nd event.

On the other hand, the SC of the traditional method reaches its limit during the 2nd LVRT event as shown in Fig. 8(b). During the unavailability of the SC, the PV needs to curtail its power generation to zero to reduce the unbalanced power on the dc-link. Meanwhile, the grid-side inverter needs to control the dc-link voltage instead of the SC. This work adopts the PV power curtailment function from [29] in which the PV's dc-dc converter is controlled by the duty cycle according to the PV power reference during the curtailment. During the control mode transition, the dc-link voltage oscillates to 1020 V before returning to its nominal value. This dc-link overvoltage can be higher in magnitude and last for a longer time if the PV needs to curtail from a higher PV power or the PV control has a slower response time than the one implemented in this paper. Consequently, the PVSS's stability might be reduced, and it might lead to the disconnection of the PVSS from the grid during a severe LVRT event.

As compared to the proposed method with sufficient SC capacity during the events, the SC can maintain the PVSS's stability as verified by the seamless transition during the LVRT events without any dc-link overvoltage issues. Meanwhile, the PV can continue its operation in MPP during the LVRT events.

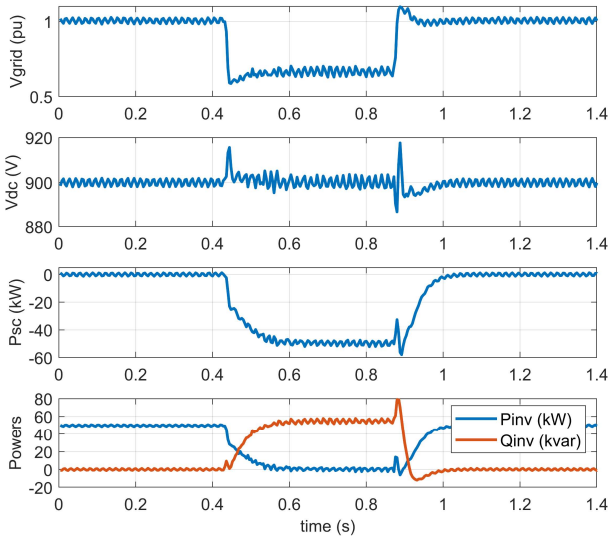

Fig. 7. Experimental results of PVSS operation under LVRT event.

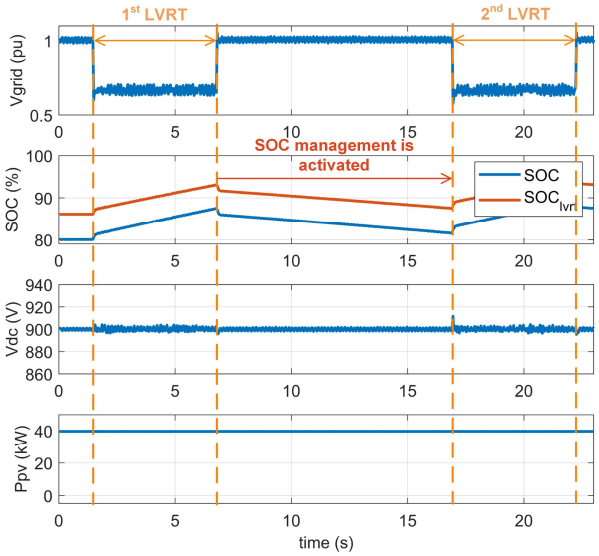

(a) Experimental results of the SOC reservation concept.

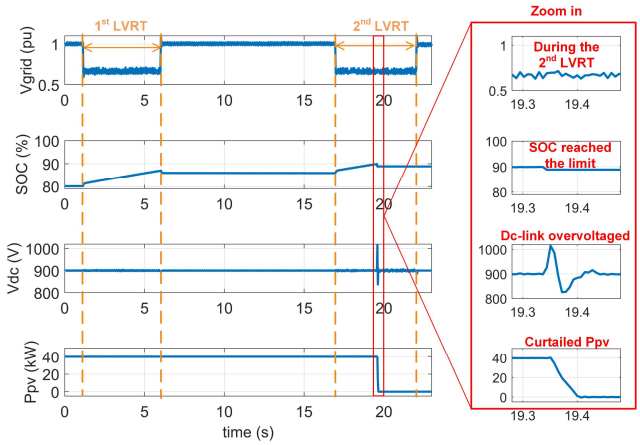

(b) Experimental results of the traditional method [1].

Fig. 8. LVRT performance of the SOC reservation concept compared to the traditional control [1].

C. Results of SOC Management

1) SC current adjustment based on SC thermal model

This study incorporates a SC thermal model to adjust the SC current during SOC management rather than adopting the constant SC current based on the SC datasheet in order to shorten the management time. The comparison results of the SOC management according to these methods when charging the SC are presented in Fig. 9.

The SC current from the model incorporating the SC temperature is higher than the limit current provided in the SC datasheet. Because the SC current is set based on the SC temperature at 25 ºC, which is relatively low compared to its upper limit at 60 ºC. Thus, the management time of the high current operation is shorter than the time when using the constant SC current. The temperature rise according to the high current operation is higher than using the constant current. However, the temperatures are not much different within the short time of the SOC management.

By incorporating the SC thermal capacity to adjust the SC operations, the tradeoff between the thermal model accuracy and the required computation time should be considered for the real-time application.

2) SOC management considering grid condition

The SOC management when considering the grid condition is demonstrated in Fig. 10. In this scenario, the PV operates at 25 kW, and the SC needs to inject power to the grid since the SOC_{lvrt} reaches its limit at 90%.

At the beginning of the SOC management, the grid voltage is close to the upper boundary, thus the power during the management is adjusted to a low value to avoid violating the grid condition. After the grid voltage is reduced close to its nominal value, the injected power is increased to the full power capacity until the SOC_{lvrt} reaches the target value at 65%.

Another scenario is demonstrated where the results of the SOC management comparing the benchmark method with the proposed method are shown in Fig. 11. The benchmark method with the traditional fixed power [1], [9], [10] is set based on its maximum power at 55 kW to quickly achieve SOC management while utilizing the disable and enable function of the SOC management based on the grid voltage conditions. Meanwhile, the proposed method adjusts the power reference during SOC management according to the grid voltage.

In this scenario, the SOC management starts from t = 5 s when the grid voltage is close to the boundary at 1.05 pu, and without any PV power generation. The SC power from the proposed method is adjusted to be at a low value of 5 kW to maintain the grid voltage within the limits. Meanwhile, using a traditional fixed SC power causes power fluctuations due to disabling and enabling SOC management from the oscillation of the grid voltage at the limit. This power fluctuation worsens the grid voltage condition which can lead to the disconnection of other nearby devices in the grid due to their undervoltage or overvoltage protection settings.

The SOC management should be considered as one of PVSS's operations in which both the PVSS's capacity and the power system condition should be considered so that the safe operations of both the grid and the PVSS can be accomplished.

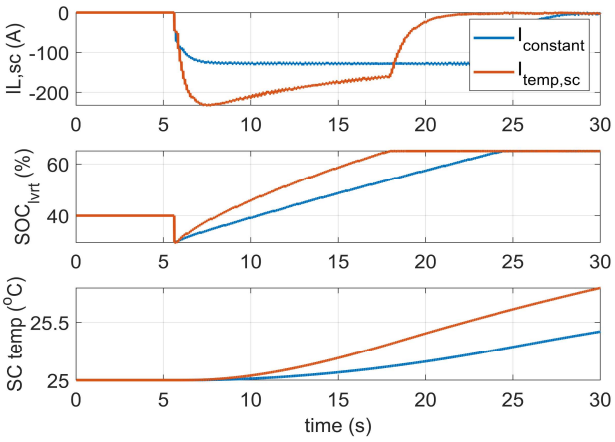

Fig. 9. Experimental results of the SOC management based on constant current (blue) and current depending on the SC temperature (red).

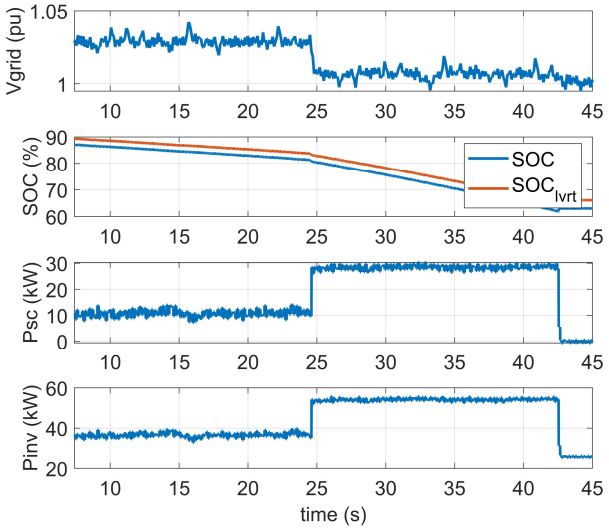

Fig. 10. Experimental results of SOC management when considering the grid voltage condition.

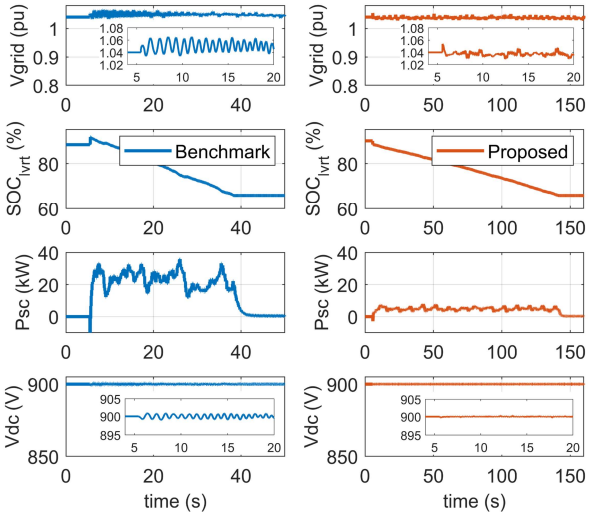

Fig. 11. Experimental results of SOC management based on the benchmark method (blue) and the proposed method (red).

VIII. Conclusions

During LVRT operations, a SC can be used to absorb or provide power to the dc-link of a grid-connected PV with a supercapacitor system (PVSS). The dc-link voltage stability of PVSS can be well regulated due to the fast response of the SC. With a limited capacity of the SC, PVSS stability can be reduced if the SC is unavailable during LVRT operations. This study proposes the SOC reservation concept for LVRT operations with SOC management that considers both grid and PVSS conditions. The proposed SOC reservation concept can ensure SC availability to provide LVRT services complying with grid code requirements while maintaining PVSS's stability during LVRT operations. Meanwhile, the proposed SOC management method can fully utilize the SC capacity according to its limits in terms of voltage, current, and temperature while ensuring the operation will not violate the grid conditions. Thus, the SOC management can be completed faster than the existing literature with the fixed power reference during normal grid conditions.

References

[1] B. R. Naidu, P. Bajpai and C. Chakraborty, "Energy storage unit for dynamic voltage support in distribution networks," in *IEEE International Conference on Power Systems (ICPS)*, Kharagpur, India, 2021, pp. 1-6.

[2] S. Karpana, E. Batzelis, S. Maiti, and C. Chakraborty, "PV-Supercapacitor cascaded topology for primary frequency responses and dynamic inertia emulation," in *Energies*, vol. 14, no. 24, p. 8347, Dec. 2021.

[3] M. Y. Worku and M. A. Abido, "Grid-connected PV array with supercapacitor energy storage system for fault ride through," in *IEEE International Conference on Industrial Technology (ICIT)*, Seville, Spain, 2015, pp. 2901-2906.

[4] M. E. Şahin and F. Blaabjerg, "A hybrid PV-battery/Supercapacitor system and a basic active power control proposal in MATLAB/ Simulink," in *Electronics*, vol. 9, no. 1, p. 129, Jan. 2020.

[5] M. C. Argyrou, C. C. Marouchos, S. A. Kalogirou, and P. Christodoulides, "Modeling a residential grid-connected PV system with battery–supercapacitor storage: control design and stability analysis," in *Energy Reports*, vol. 7, pp. 4988–5002, Nov. 2021.

[6] G. Navarro, J. Torres, M. Blanco, J. Nájera, M. Santos-Herran, and M. Lafoz, "Present and future of supercapacitor technology applied to powertrains, renewable generation and grid connection applications," in *Energies*, vol. 14, no. 11, p. 3060, May 2021.

[7] I. Hamdan, A. Maghraby, and O. Noureldeen, "Stability improvement and control of grid-connected photovoltaic system during faults using supercapacitor," in *SN Applied Sciences*, vol. 1, no. 12, pp. 1–19, 2019.

[8] Maxwell Technologies, "Product Guide Maxwell Technologies: BOOSTCAP Ultracapacitor," 2009. [Online]. Available: https://maxwell.com/products/ultracapacitors/downloads/

[9] G. Rancilio, A. Rossi, C. Di Profio, M. Alborghetti, A. Galliani, and M. Merlo, "Grid-scale BESS for ancillary services provision: SoC restoration strategies," in *Applied Sciences*, vol. 10, no. 12, p. 4121, Jun. 2020.

[10] C. Jamroen, S. Sirisukprasert, and N. Hatti, "A study on SOC management of energy storage system for voltage regulation application in distribution network," in *International Renewable Energy Congress (IREC)*, Hammamet, Tunisia, 2020.

[11] S. Y. Yu, H. J. Kim, J. H. Kim, and B. M. Han, "SoC-based output voltage control for BESS with a lithium-ion battery in a stand-alone dc microgrid," in *Energies*, vol. 9, no. 11, p. 924, Nov. 2016.

[12] P. Kritprajun et al., "Development of a converter-based supercapacitor system emulator for PV applications." in *IEEE Energy Conversion Congress and Exposition*, Nashville, TN, USA, 2023.

[13] H. Miniguano, A. Barrado, C. Fernández, P. Zumel, and A. Lázaro, "A general parameter identification procedure used for the comparative study of supercapacitors models," in *Energies*, vol. 12, no. 9, May 2019.

[14] D. Somayajula and M. L. Crow, "An ultracapacitor integrated power conditioner for intermittency smoothing and improving power quality of distribution grid," in *IEEE Transactions on Sustainable Energy*, vol. 5, no. 4, pp. 1145-1155, Oct. 2014.

[15] J. Sun, S. Wang, J. Wang and L. M. Tolbert, "Dynamic model and converter-based emulator of a data center power distribution system," in *IEEE Transactions on Power Electronics*, vol. 37, no. 7, pp. 8420-8432, July 2022.

[16] Mathwork, "400-kW grid-connected PV farm (average model)," June 2023. [Online]. Available: https://www.mathworks.com/help/sps/ug/400-kw-grid-connected-pv-farm-average-model.html

[17] W. Wang, A. Beddard, M. Barnes and O. Marjanovic, "Analysis of active power control for VSC–HVDC," in *IEEE Transactions on Power Delivery*, vol. 29, no. 4, pp. 1978-1988, Aug. 2014.

[18] "IEEE Standard for Interconnection and Interoperability of Distributed Energy Resources with Associated Electric Power Systems Interfaces," in IEEE Std 1547-2018 (Revision of IEEE Std 1547-2003), pp.1-138, 6 April 2018.

[19] J. M. Miller, "Ultracapacitor modeling," in *Ultracapacitor Applications*, The Institution of Engineering and Technology, Stevenage, 2011.

[20] B. Pozo, J. Garate, S. Ferreiro, I. Fernandez, and E. Fernandez de Gorostiza, "Supercapacitor electro-mathematical and machine learning modelling for low power applications," in *Electronics*, vol. 7, no. 4, p. 44, Mar. 2018.

[21] Maxwell Technologies, "2.7V 3000F ULTRACAPACITOR CELL," BCAP3000 P270 K04/05 datasheet, 2022. [Online]. Available: https://maxwell.com/wp-content/uploads/2022/11/3003279-EN.3_DS_2.7V-3000F-Cell-BCAP3000-P270.pdf

[22] V. Lystianingrum, B. Hredzak, V. G. Agelidis and V. S. Djanali, "On estimating instantaneous temperature of a supercapacitor string using an observer based on experimentally validated lumped thermal model," in *IEEE Transactions on Energy Conversion*, vol. 30, no. 4, pp. 1438-1448, Dec. 2015.

[23] S. Hamedi, T. Ghanbari, Z. Hosseini, E. Moshksar, "Self-discharge estimation of supercapacitor modules at different ventilation levels," in *Journal of Energy Storage*, vol. 52, 2022.

[24] A. Hijazi, P. Kreczanik, E. Bideaux, P. Venet, G. Clerc and M. Di Loreto, "Thermal network model of supercapacitors stack," in *IEEE Transactions on Industrial Electronics*, vol. 59, no. 2, pp. 979-987, Feb. 2012.

[25] X. Lin, H. Fu, H.E. Perez, J.B. Siege, A.G. Stefanopoulou, Y. Ding, M.P. Castanier, "Parameterization and observability analysis of scalable battery clusters for onboard thermal management," in *IFP Energies nouvelles International Conference*, 2013, pp. 165–178.

[26] I. Zupan, V. Sunde, Z. Ban, and D. Kruselj, "Algorithm with temperature-dependent maximum charging current of a supercapacitor module in a tram regenerative braking system," in *Journal of Energy Storage*, vol. 36, 2021.

[27] L. Yang et al., "Three-phase power converter-based real-time synchronous generator emulation," in *IEEE Transactions on Power Electronics*, vol. 32, no. 2, pp. 1651-1665, Feb. 2017.

[28] J. Wang et al., "Static and dynamic power system load emulation in converter-based reconfigurable power grid emulator," in *IEEE Energy Conversion Congress and Exposition*, Pittsburgh, PA, USA, 2014.

[29] Y. Zhu, H. Wen, G. Chu, Y. Hu, X. Li and J. Ma, "High-performance photovoltaic constant power generation control with rapid maximum power point estimation," in *IEEE Transactions on Industry Applications*, vol. 57, no. 1, pp. 714-729, 2021.